3. PERFORMANCE CHARACTERISTICS OF A JET-FLAP ROTOR

By John L. McCloud III, William T. Evans,
and James C. Biggers
Ames Research Center

SUMMARY

Results of an experimental investigation of the characteristics of a jet-flap rotor are presented and discussed. Comparisons of the rotor's force-producing capabilities with those of a conventional rotor are made which show the jet-flap rotor to be operable well beyond standard rotor stall boundaries. Correlations are made between measured and calculated results which show generally good agreement.

Author

INTRODUCTION

As a part of NASA's VTOL investigations, various methods of increasing the forward speed capabilities of helicopter rotors are being studied. Rotor forward speeds are aerodynamically limited by retreating blade stall, a decreasing ability to develop propulsive force loads at high advance ratios without extreme rotor tilting, and compressibility effects which occur on the advancing blade tips. One method of avoiding these problems is by application of jet flaps to the helicopter rotor blades. The jet-induced "supercirculation" and BLC effects may delay the stall, permitting large propulsive and lifting loads at high forward speeds.

This type of rotor has been studied analytically and reported in references 1, 2, and 3. The French firm of Giravions Dorand has built such a rotor under contract to the U. S. Army, and this rotor has been tested in the Ames 40- by 80-foot wind tunnel. The jet-flap rotor was driven and controlled by the jet itself. The blades were fixed in pitch and varying the jet-flap deflection angle, both cyclically and noncyclically, controlled the rotor force output.

Data were obtained at hover and forward flight conditions corresponding to advance ratios of 0.3, 0.4, and 0.5 for two blade angle settings. Data presented here compare the jet-flap rotor's force-producing capability with a conventional rotor's stall boundaries. Data showing correlation with calculated performance, obtained by the digital computation methods of reference 1, are also presented.

NOTATION

$\bar{A}_0$ collective jet deflection, deg

$\bar{B}_1$ cyclic jet deflection, deg, $\theta_j = \bar{A}_0 - \bar{B}_1 \sin \psi$

b number of blades

C_{j_R} rotor jet-momentum coefficient, $\frac{M_j V_j}{\rho(\Omega R)^2 \pi R^2}$

C_{L_R} rotor lift coefficient, $\frac{L}{\rho(\Omega R)^2 \pi R^2}$

C_{X_R} rotor propulsive-force coefficient, $\frac{X}{\rho(\Omega R)^2 \pi R^2}$

c blade chord, ft

c_e equivalent blade chord (on thrust basis), $\frac{\int_{0.111R}^{0.99R} cr^2 dr}{\int_{0.111R}^{0.99R} r^2 dr}$, ft

L lift, lb

M_j total mass flow through both blades, slugs/sec

R rotor radius, ft

r radius station, ft

V free-stream velocity, ft/sec

V_j jet velocity, assuming adiabatic expansion from blade duct pressure, ft/sec

$\frac{V}{\Omega R}$ advance ratio

X propulsive force, positive upstream, lb

α_s shaft angle, positive rearward from vertical, deg

θ_j jet deflection, positive downward from chord line, deg

θ blade angle, relative to tip chord line, deg

$\theta_{0.7}$ collective pitch of blade at 0.7R, deg

ρ free-stream air density, slugs/ft^3

σ rotor solidity, $\frac{bc_e}{\pi R}$

ψ blade azimuth angle, measured from downstream in direction of rotation, deg

Ω rotational speed of rotor, rad/sec

MODEL AND APPARATUS

Rotor

Figure 1 shows the rotor and air supply unit installed in the wind tunnel. The rotor was two-bladed, with offset coning hinges and a central teetering hinge. Twist distribution, planform, and airfoil sections of the blades are illustrated in figure 2. A linear twist distribution of -8° is shown for comparison purposes. The blades for these tests had no feather bearings and were fixed in pitch. Tests were made at blade pitch settings of $\theta_{0.7} = 8^\circ$ and 12°. The inboard portion of the blade out to the 0.4R station has elliptical cross sections. The blade has constant chord and thickness from 0.4R to 0.7R and then tapers in both chord and thickness from 0.7R to the tip. The jet flap and nozzle also begin at 0.7R and extend to the blade tip.

The fixed pitch setting of the test rotor is not requisite to the jet-flap principle, but, pending results of application studies, it could be a desirable feature made possible by the jet flap. The other details of the rotor, with the possible exception of thickness, are also not dictated by the jet flap.

The details of the jet flap are shown in figure 3. The compressed air was ducted through the blade spar and then, by a cascade of turning vanes, was exhausted out the trailing portion of the blade over a short mechanical flap. Mechanically deflecting the flap deflects the jet flow as the air follows the upper surface by the Coanda effect. The flow out the nozzle provides the torque for rotor rotation, and deflecting the jet flap cyclically and noncyclically controls the rotor's force output.

The mechanical portion of the flap was deflected by a pneumatic system which was controlled by a swash plate and linkage system. The swash plate, housed in the cylindrical portion of the hub, was positioned by electric actuators (see fig. 4).

Rotor Support System

The rotor suspension shown in figure 4 consisted of a three-legged, spring-loaded parallelogram system. This system provided inplane softness, longitudinal and lateral, without changing the tilt of the rotor shaft. The parallelogram structure was supported in turn by a strain-gage balance platform which

pivoted about point A of figure 4. This pivoting action, which tilts the shaft axis, was controlled by an electric actuator not shown.

The air ducting to the rotor is split to provide two opposing flows to the rotor. This is necessary since the air source is mounted below the balance platform. A universal joint in the ducting accepts these two flows and provides the articulation necessary for shaft-axis tilt.

The rotor suspension system was shielded from air loads by a fairing (see fig. 1) attached to the support system below the strain-gage platform. However, the fairing "cap" was attached to the upper portion of the parallelogram system; hence its air loads were sensed by the strain-gage balance. The drag load of this "cap" and that of the hub, slip rings, etc., have been removed from the data herein as tares.

The compressed air to drive the rotor was supplied by an axial-flow compressor driven by a constant-speed turboshaft engine. The amount of air supplied to the rotor was set by control valves at the compressor outlet (point B of fig. 4).

Instrumentation

All rotor forces and moments were measured by the six-component strain-gage balance system previously discussed. The compressed air-flow rate was measured by an orifice meter in the vertical air-supply line downstream of the flow-control valves. Compressed air temperature was measured at this point. Additional pressures and temperatures and several rotor-blade stresses, hinge motions, and vibration levels were monitored during the investigation.

RESULTS AND DISCUSSION

The basic results of the wind-tunnel tests are shown in figure 5. For the conditions indicated, these plots show the lift and propulsive force coefficients developed by the jet-flap rotor at advance ratios of 0.30 and 0.51. Also indicated on these plots are retreating blade stall limits for a standard rotor. Specifically, these limits correspond to the upper stall boundaries of a rotor having -8° of twist as obtained from the charts of reference 4. Conventional rotors must be operated at force levels below these limits to avoid retreating blade stall. The increased load-carrying capability of the jet-flap rotor is quite substantial, reaching as high as 2 to 2-1/2 times the capability of a conventional rotor. These loads would not have been achieved without the increased lift due to the circulation and BLC effects of the jet flap. The higher force values were limited by the test rotor's mechanical limitation to a maximum jet-flap deflection of approximately 50°. (Note that $\overline{A}_0 + \overline{B}_1 = 46^{\circ}$ for the data of fig. 5.)

The high force capability of the jet-flap rotor is compared in figure 6 to that for a conventional rotor over a range of flight speeds from 0 to 300 knots.

In this instance the highest values of jet-flap rotor lift have been made dimensionless by dividing by the static thrust obtainable from a conventional rotor for the same tip speeds and areas, etc.[1] The upper limit of lift capability for the conventional rotor at forward speeds is based on the retreating blade stall criteria previously stated. The specific value of $V/\Omega R$ for which the conventional rotor can no longer develop any lift at all depends upon its propulsive force requirement (ref. 5).

The jet-flap rotor's experimentally demonstrated capability is indicated by the data points, of which two correspond to the high propulsive force conditions of figure 5. From hover to an advance ratio of 0.5 the increased lift capability is substantial. The data for the jet-flap rotor do not represent flight limits. There were no indications of retreating blade stall, and even higher forces and advance ratios might have been attained with a greater range of flap deflections.

Also indicated on this figure is a region representing lift and forward speed conditions for which performance has been calculated. These calculations are based on the special analyses for jet-flap rotors reported in reference 1. The calculations were made on digital computing machines and include the necessary inputs to account for compressibility and reverse flow effects. Note that calculated performance for the jet-flap rotor indicates a significant rotor force capability at forward speeds up to 300 knots. At this speed conventional rotors must be unloaded by compounding, that is, by the addition of wings and propulsion units to the aircarft.

COMPARISON WITH THEORY

Collective Variation

The large forces developed and the high forward speeds indicated as obtainable by the jet-flap rotor make it desirable to compare measured and calculated performance in more detail. Figure 7 shows such a comparison. Examination of both portions of the figure shows the calculated and measured data to compare very favorably in an overall qualitative sense. There are some slope differences and, hence, the degree of quantitative agreement depends on the conditions chosen for comparison. It may be noted that the data shown in figure 7 are similar to those for a conventional rotor. The variation of C_{L_R} versus C_{X_R} as shaft angle changes (at constant jet collective) is similar to the variation of C_{L_R} versus C_{X_R} as shaft angle (or control axis inclination) changes at a constant collective blade pitch setting for a conventional rotor. The variations of C_{L_R} and C_{X_R} with jet collective changes at constant shaft angles are also similar to those due to blade collective pitch changes on a conventional rotor.

---

[1]Static thrust obtainable is based on a $C_{L_R}/\sigma = 0.16$, which is indicated by reference 4 as a probable upper limit.

Cyclic Variation

The measured and calculated effects of cyclic deflection of the jet flap are shown in figure 8. The data are for various shaft angles of attack and cyclic jet deflections at fixed collective jet deflections.

For a conventional rotor, increasing blade cyclic pitch at constant collective pitch and shaft angle of attack produces C_{L_R} versus C_{X_R} variations similar to those shown for the shaft angle variation. However, increasing jet-flap cyclic deflections increases propulsive force coefficient with little change in lift coefficient.

Again, the calculated variation shows the same general effects as the measured data, and again there are differences in details. For example, the measured data show slight lift increases with increased cyclic jet-flap deflection whereas the calculations show slight decreases.

Data for other blade angles and advance ratios show the same degree of correlation.

Momentum Requirements

Figure 9 shows the momentum requirements for the rotor at the conditions indicated. These data correspond to the data of figure 7. The changes in momentum coefficient C_{j_R} shown in figure 9 reflect the changes in propulsive force coefficient shown in figure 7. The calculated C_{j_R} variations are quite similar to the measured variations although the general level of the measured values is higher. The increment between measured and calculated C_{j_R} values was fairly consistent for all test conditions. For example, figure 10, which shows data obtained for hover conditions, has similar increments. The calculations did not take into account any nozzle losses or thrust losses due to the jet flow over the mechanical portion of the flap, which probably accounts for these differences.

Comparison of equivalent shaft power for the jet-flap rotor with that for a conventional rotor depends upon the conditions chosen. When the conventional rotor is unstalled, the jet-flap rotor requires more power, as discussed in reference 1. When the increased lift capability of the jet-flap rotor is utilized, the extra power required is diminished. At speeds above 200 knots, the conventional rotor can no longer develop lift and propulsive loads; hence shaft power comparisons become meaningless.

CONCLUDING REMARKS

Wind-tunnel tests have been made of a two-bladed rotor, driven and controlled by a jet flap incorporated in the outer 30-percent radius of each blade. The rotor produced very large lift and propulsive forces, indicating that

jet-flap high-lift phenomena can be utilized on a helicopter rotor blade. High advance ratios were reached without indications of retreating blade stall, and the large forces produced per unit blade area exceeded conventional rotor capabilities by factors of 2 and more.

Varying the jet deflection angle, cyclically and noncyclically, was shown to control and direct the rotor's force. Comparisons of measured and calculated characteristics show the calculation method to give generally good correlations. Additional investigations with the test rotor's mechanical limitations removed are needed to evaluate this correlation at even higher advance ratios and at conditions where compressibility effects occur.

The increased lift and propulsive force capabilities shown, which did not represent jet-flap concept limits, indicate the jet-flap rotor to be both feasible and of potential value for high-speed rotors, low or moderate speed rotors where high lift is required, or for helicopters where the high lift per unit area may be utilized to reduce the rotor size.

REFERENCES

1. Evans, William T.; and McCloud, John L., III: Analytical Investigation of a Helicopter Rotor Driven and Controlled by a Jet Flap. NASA TN D-3028, 1965.

2. Dorand, René; and Boehler, Gabriel D.: Application of the Jet-Flap Principle to Helicopters. J. Am. Helicopter Soc., vol. 4, no. 3, July 1959, pp. 26-36.

3. Greenman, R. N.; and Gaffney, M. G.: Application of Circulation Control to Helicopter Rotors. Rep. ARD 158, Hiller Helicopter Co., 1957.

4. Tanner, Watson H.: Charts for Estimating Rotary Wing Performance in Hover and at High Forward Speeds. NASA CR-114, 1964.

5. Fradenburgh, Evan A.; and Segel, Richard M.: Model and Full Scale Compound Helicopter Research. Presented at the American Helicopter Society, Twenty-First Annual National Forum, Washington, D. C., May 12-14, 1965.

JET-FLAP ROTOR IN WIND TUNNEL

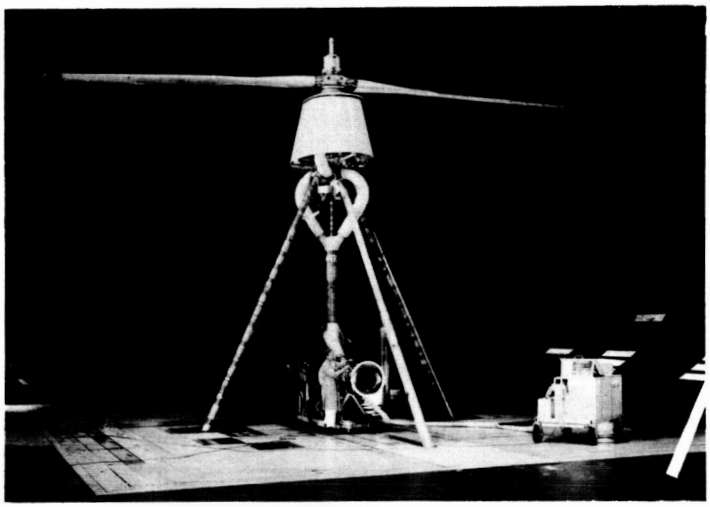

Figure 1 A-34959.1

JET-FLAP ROTOR

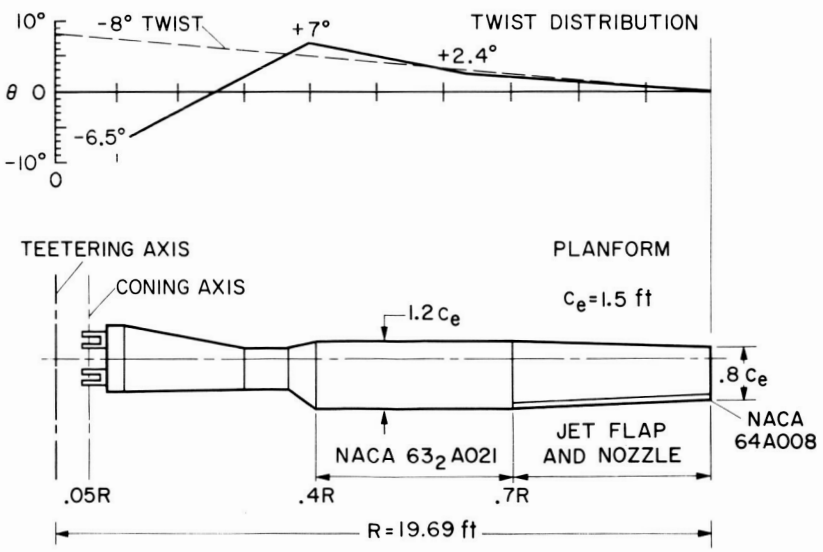

Figure 2

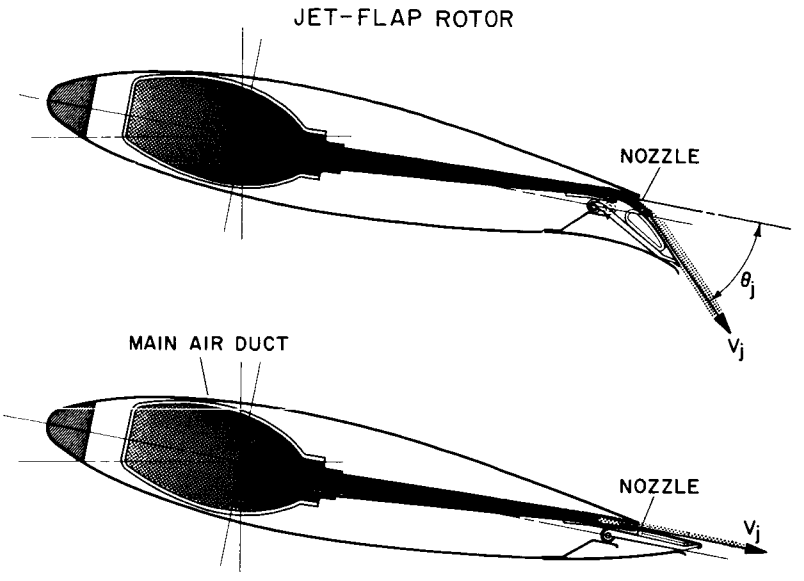

Figure 3

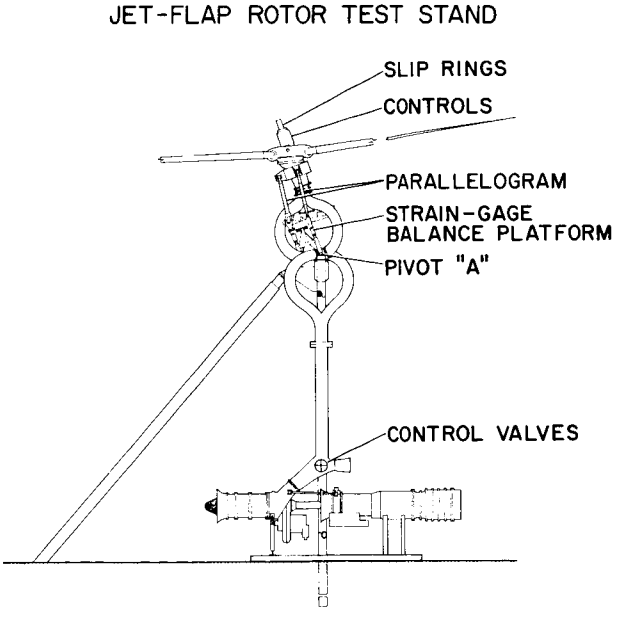

Figure 4

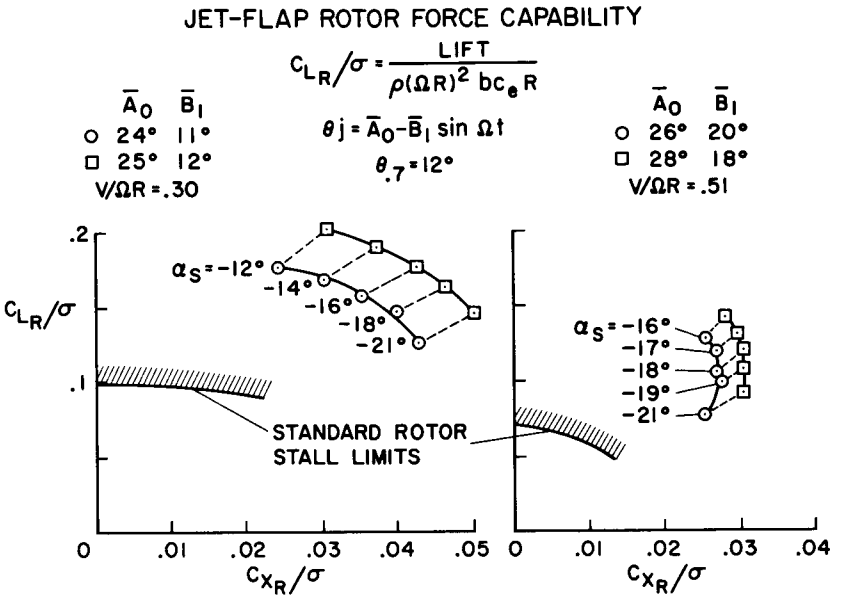

Figure 5

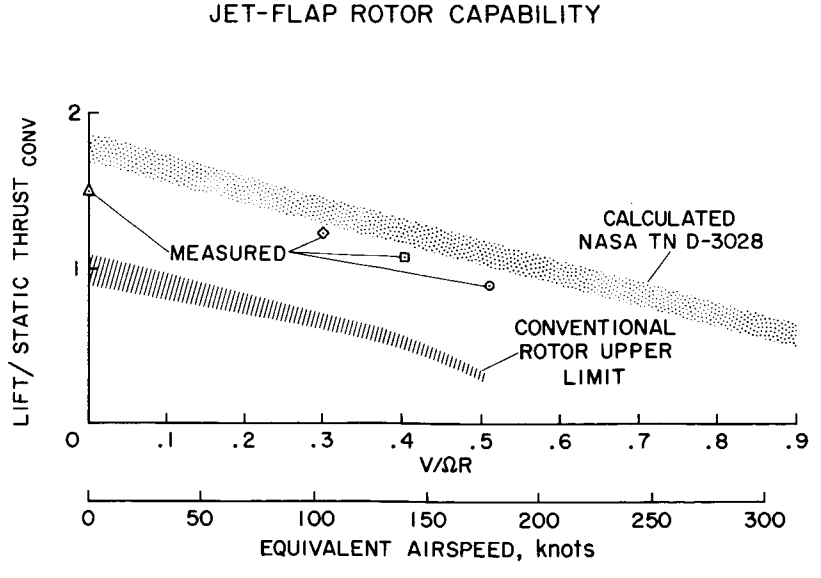

Figure 6

COMPARISON WITH THEORY – COLLECTIVE VARIATION

$\theta_{.7} = 8°$ $V/\Omega R = .30$

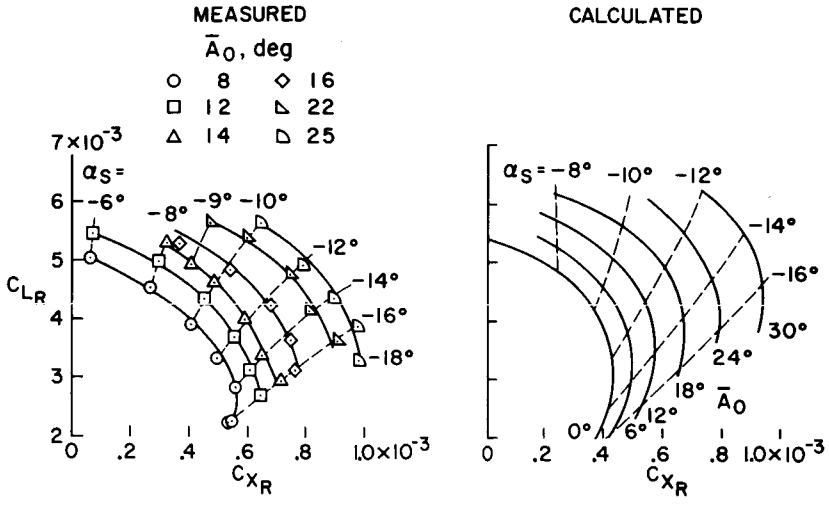

Figure 7

COMPARISON WITH THEORY – CYCLIC VARIATION

$\theta_{.7} = 8°$ $V/\Omega R = .30$

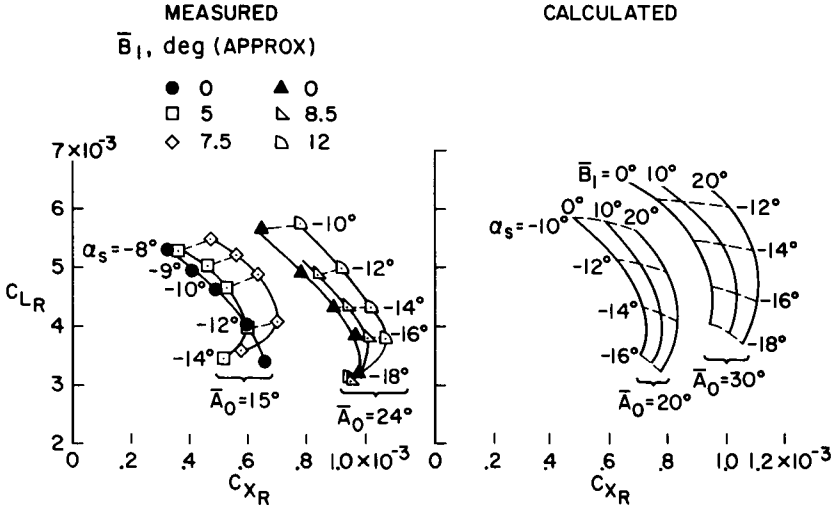

Figure 8

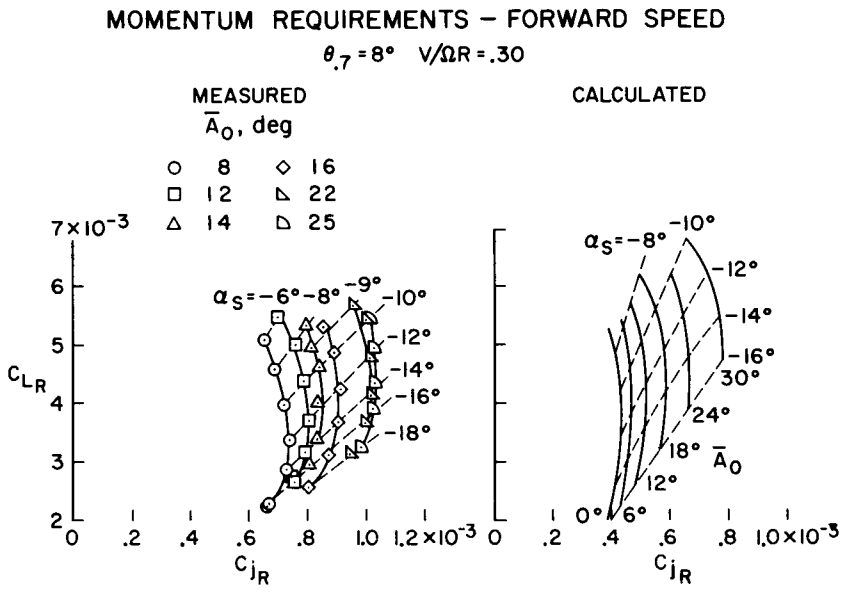

Figure 9

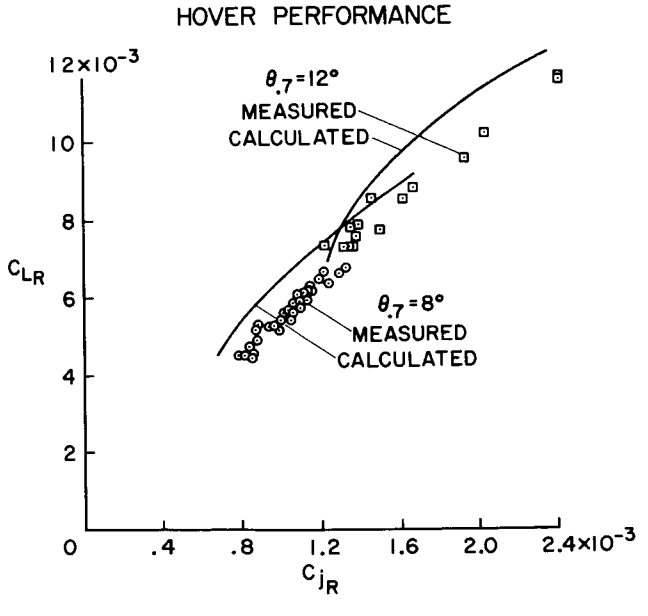

Figure 10